Chromite-hosted Silicate Melt Inclusions from Basalts in the Stravaj Complex, Southern Mirdita Ophiolite Belt (Albania)

IZABELLA HAVANCSÀK

FRIEDRICH KOLLER

JÀNOS KODOLÀNYI

CSABA SZABÒ

VOLKER HÖCK

See next page for additional authors

Recommended Citation

Chromite-hosted Silicate Melt Inclusions from Basalts in the Stravaj Complex, Southern Mirdita Ophiolite Belt (Albania)

Authors

IZABELLA HAVANCSÀK, FRIEDRICH KOLLER, JÀNOS KODOLÀNYI, CSABA SZABÒ, VOLKER HÖCK, and KUJTIM ONUZI

Chromite-hosted Silicate Melt Inclusions from Basalts in the Stravaj Complex, Southern Mirdita Ophiolite Belt (Albania)

IZABELLA HAVANCSÁK[1], FRIEDRICH KOLLER[2], JÁNOS KODOLÁNYI[3],
CSABA SZABÓ[1], VOLKER HOECK[4,5] & KUJTIM ONUZI[6]

[1] Department of Petrology and Geochemistry, Lithosphere Fluid Reseach Lab, Institute of Geography and Earth Sciences, Eötvös University, Pázmány P. sétány 1/c, H-1117 Budapest, Hungary
[2] Department of Lithospheric Research, University of Vienna, Geocenter, Althanstr. 14, A-1090 Vienna, Austria (E-mail: friedrich.koller@univie.ac.at)
[3] Institute of Geological Sciences, University of Bern, Baltzerstrasse 1-3, CH-3012 Bern, Switzerland
[4] Department of Geography and Geology, University of Salzburg, Hellbrunnerstr. 34, A-5020 Salzburg, Austria
[5] Department of Geology, Babes-Bolyai University, Kogalniceanu Str. 1, RO-400084 Cluj-Napoca, Romania
[6] Instituti i Gjeoshkencave, Universiteti Politeknik i Tiranes, Albania

Abstract: The Stravaj ophiolite compex, part of the western Mirdita ophiolite belt in Albania, is located east of the Shpati massif, and west of the Shebenik massif. The Stravaj ophiolite sequence itself consist of MOR-related and subduction-related volcanic rocks (Hoeck *et al.* 2007) formed by pillow lavas and various dykes. The deeper units are formed by gabbros and plagioclase-bearing peridotites. The pillow lavas are intersected by basaltic dykes with a rather primitive composition.

The studied basaltic dyke contains former relics of olivine, fresh spinel and clinopyroxene phenocrysts in a glassy groundmass. The silicate phases are strongly altered. The spinels appear as fresh, opaque grains preserved in totally altered olivine phenocrysts. The spinels host negative crystal shaped, multiphase silicate melt inclusions. The inclusions consist commonly of clinopyroxene daughter minerals, glass and rare sulphide blebs.

A series of heating experiments were conducted, using the furnace technique to homogenize the silicate melt, in order to obtain homogenized silicate melt inclusions for major and trace element composition analysis and to determine their homogenization temperatures. Therefore, samples were heated to and quenched from 1200±20°C to 1240°C. The melt inclusions homogenized between 1220–1240±20°C. The major element composition of the homogenized melt inclusions is 48.3–51.2 wt% SiO_2, 5.4–6.7 wt% FeO, 9.9–12.6 wt% MgO, 14.5–17.3 wt% Al_2O_3, 1.9–2.4 wt% Na_2O and 12.1–13.0 wt% CaO. This result is highly comparable with the host mafic rock composition. The trace element composition of the homogenized silicate melt shows characteristic LREE-depleted patterns (La: 0.24–0.35 ppm), while the MREE and HREE patterns are generally flat: average PM-normalized La/Lu is 0.094. The average contents of compatible trace elements such as Cr, Ni, V, Co are up to 621 ppm, 825 ppm, 235 ppm and 80 ppm, respectively.

Based on the major composition, trace element characteristics and the calculated oxygen fugacity, the studied silicate melt inclusions show strong similarities to MOR-related volcanic rocks found commonly in the Stravaj Massif. These chromite-bearing basalt dykes define extreme primitive MORB related melts in the upper part of the pillow lava section.

Key Words: ophiolite, chromite, basalt, melt inclusions, Albania

Stravaj Karmaşığı'ndaki Bazaltlardaki Kromitler içindeki Silikat Sıvı Kapanımları, Güney Mirdita Ofiyolit Kuşağı (Arnavutluk)

Özet: Arnavutluk'taki Batı Mirdita Ofiyolit Kuşağı'nın bir parçası olan Stravaj ofiyolit kompleksi, Shpati masifinin doğusunda ve Shebenik masifinin batısında yeralmaktadır. Stravaj ofiyolit serisi, yastık lavlar ve çeşitli dayklardan oluşan okyanus ortası sırtı ve dalma-batma ile ilgili volkanik kayaçları içermektedir (Hoeck vd. 2007). Derindeki birimler, gabrolar ve plajiyoklas içeren peridotitlerdir. Yastık lavlar nispeten daha birincil bileşimdeki bazalt daykları ile kesilmektedir.

Çalışılan bazalt daykları, camsı hamur içinde öncel olivin kalıntıları, taze spinel ve klinopiroksen fenokristalleri içermektedir. Silikat fazları oldukça altere olmuştur. Spineller negatif kristal şekilli, çoklu-fazlı silikat sıvı kapanımları içerir. Bu sıvı kapanımları, genel olarak, klinopiroksenden türemiş mineraller, cam ve az miktarda sülfid kabarcıklarıdır.

Ana ve iz element bileşim analizlerinin yapılabilmesi ve homojenleşme sıcaklığının belirlenebilmesi amacıyla, silikat eriyiğinin homojenleştirilmesi için fırın kullanılarak bir dizi ısıtma deneyi uygulanmıştır. Böylece örnekler, 1200°C ± 20°C 'den 1240°C 'ye ısıtılmış ve söndürülmüştür. Sıvı kapanımları, 1200°C ± 20°C ile 1240°C arasında homojenleşmiştir. Homojenleşmiş eriyiğin ana element içerikleri; 48.3–51.2 wt% SiO_2, 5.4–6.7 wt% FeO, 9.9–12.6 wt% MgO, 14.5–17.3 wt% Al_2O_3, 1.9–2.4 wt% Na_2O ve 12.1–13.0 wt% CaO şeklindedir. Bu sonuç, ana mafik kayaç bileşimiyle oldukça uyumludur. Homojenleşmiş silikat eriyiğin iz element içerikleri, karakteristik hafif NTE-fakir dağılımlar gösterirken (La: 0.24–0.35 ppm), ortaç NTE ve ağır NTE dağılımları genel olarak düz olup, ortalama birincil mantoya gore normalize edilmiş La/ Lu oranı ise 0.094'tür. Krom, Ni, V ve Co gibi uyumlu iz elementlerin ortalama içerikleri sırasıyla, 621 ppm, 825 ppm, 235 ppm ve 80 ppm'e kadar çıkmaktadır.

Ana bileşim, iz element özellikler ve hesaplanmış oksijen fugasitesine dayanarak, çalışılan silikat sıvı kapanımları, Stravaj masifinde genellikle bulunan, okyanus ortası sırtı ile ilgili volkanik kayalara önemli benzerlikler göstermektedir. Bu kromit içeren bazalt daykları, yastık lav diziliminin üst bölümlerindeki uç birincil okyanus ortası sırtı eriyiklerini tanımlamaktadır.

Anahtar Sözcükler: ofiyolit, kromit, bazalt, sıvı kapanımları, Arnavutluk

Introduction

Melt inclusions in igneous rocks provide useful information about the temperature and pressure path and the evolution of the composition of a magmatic system (Lowenstern 1995; Frezzotti 2001; Danyushevsky *et al.* 2002). Silicate melt inclusions hosted in the first crystallizing phases (olivine and/ or spinel) represent droplets of primitive basic magma, and provide information about the source region, partial melting and fractionation of the parent magma of the studied rock (e.g., Nielsen *et al.* 1995; Danyushevsky *et al.* 2000; Norman *et al.* 2002; Zajacz *et al.* 2007; Sadofsky *et al.* 2008). In the geological literature a large database is available on silicate melt inclusions of basic effusive volcanic rocks principally hosted in olivine, pyroxene and plagioclase phenocrysts (e.g., Roedder 1984, 1987; Nielsen *et al.* 1995; Sobolev 1996; Kamenetsky *et al.* 2001; Danyushevsky *et al.* 2002; Rapien *et al.* 2003; Schiano & Clocchiatti 1994; Kóthay *et al.* 2005; Sharygin *et al.* 2007; Zajacz *et al.* 2007; Sadofsky *et al.* 2008), although spinel-hosted silicate melt inclusions have rarely been studied previously (Kamenetsky 1996; Lenaz *et al.* 2000; Kamenetsky *et al.* 2001; Spandler *et al.* 2007). The significance of silicate melt inclusions trapped in spinels is that they represent the composition of the primary magma, which was trapped, and they offer a snapshot of the magmatic system at an initial evolution-stage. The composition of spinels in basic rocks is a complex function of magma composition and other intensive parameters (e.g., T, fO_2) and they provide useful information about petrogenetic aspects, early stage magma processes and the melt source region (e.g.,

Irvine 1965, 1967; Dick & Bullen 1984; Allan *et al.* 1988; Ballhaus *et al.* 1991; Arai 1992; Kamenetsky *et al.* 2001).

In this work we have studied spinel-hosted melt inclusions from basalt dykes from the Stravaj massif (Mirdita Ophiolite Belt, Albania) to determine the origin of the studied basalt dykes. The Mirdita Ophiolite Belt consists of both MORB-like mafic sequences, and subduction-related mafic rocks (e.g., Shallo 1994; Bortolotti *et al.* 2002; Hoeck *et al.* 2002; Dilek *et al.* 2005, 2008; Koller *et al.* 2006). The aim of this study is to determine the mid-ocean ridge or subduction origin of the studied basalt dykes, using petrogenetic information from spinel-hosted silicate melt inclusions. Basic-ultrabasic rocks in ophiolite sequences often suffer low-grade ocean-floor metamorphism, so some rock-forming minerals are often altered or absent (Mevel 2003; Iyer *et al.* 2008). Contrarily, spinels are prone to most altering effects which occur during and after natural cooling and crystallization processes, and therefore are useful for geochemical investigations (Barnes 2000; Barnes & Roeder 2001). In the studied sample only spinels and their silicate melt inclusions are the primary source of information on the composition of the basalt dykes, their source rocks and crystallization processes because most of the other rock forming phases are completely or partially altered.

Geological Background of the Mirdita Ophiolite Belt

The Eastern Mediterranean region is characterized by several ophiolite belts, which can be continuously

traced from Serbia, throughout Bosnia, Macedonia, Albania, and Greece to Turkey. The ophiolites are interpreted as remnants of the Mesozoic oceanic lithosphere derived from the Neotethyan oceanic basin. The Mirdita Ophiolite Belt (Pindos in Greece) is part of this large NNW–SSE-striking ophiolite zone (see ISPGJ-FGJM-IGJN 1983: Geological map of Albania), which includes, among others, the Dinaric and Hellenic ophiolites. The Dinaric-Hellenic ophiolite zone is composed of several westward-verging ophiolite outcrops. The total length of the zone is approximately 1000 km from the Dinaric ophiolites to the Hellenic ophiolites (Pamić *et al.* 2002).

Within Albania the ophiolites are part of the Mirdita zone (Figure 1a). The ophiolite complexes in southern Albania are shown in Figure 1b. Commonly the Mirdita Ophiolite Belt is divided into two parts: (1) a western MORB belt and (2) an eastern supra-subduction zone (SSZ) belt (Figure 1b), with different petrographic and geochemical features (Shallo 1992; Bortolotti *et al.* 1996; Cortesogno *et al.* 1998; Robertson & Shallo 2000). The two belts are separated in southern Albania by the Palaeogene

and Neogene molasse sediments of the Neohellenic or Albanian-Thessalian trough (Meco & Aliaj 2000; Robertson & Shallo 2000; Hoeck *et al.* 2002; Dilek *et al.* 2005) (Figure 1a, b).

The ophiolites of the eastern belt are characterized by thick harzburgitic tectonites, followed by dunite and pyroxenite cumulates (plagiogranites, gabbros). Above the cumulates is a well-developed sheeted dyke complex, covered by volcanic sequences (pillow lavas, with basalts, andesitic and rhyodacitic rocks). The ophiolites in the western belt consist of harzburgitic and lherzolitic tectonites (including plagioclase-bearing lherzolite and dunitic cumulates). The sheeted dyke complex member of the series is usually undeveloped. A thin troctolite and gabbro complex is overlain by basaltic pillow lavas (Hoeck *et al.* 2002).

Until recently, the Mirdita Belt ophiolites were interpreted to be a composite of a MORB (mid-ocean ridge basalt) dominated western belt and a SSZ (supra-subduction zone related rocks)-type eastern belt, based on petrographic and geochemical evidences (Beccaluva *et al.* 1994; Bortolotti *et al.* 1996). The geochemical characteristics of the eastern ophiolites suggest a subduction origin, despite the sparse occurrence of MOR-related rocks described in
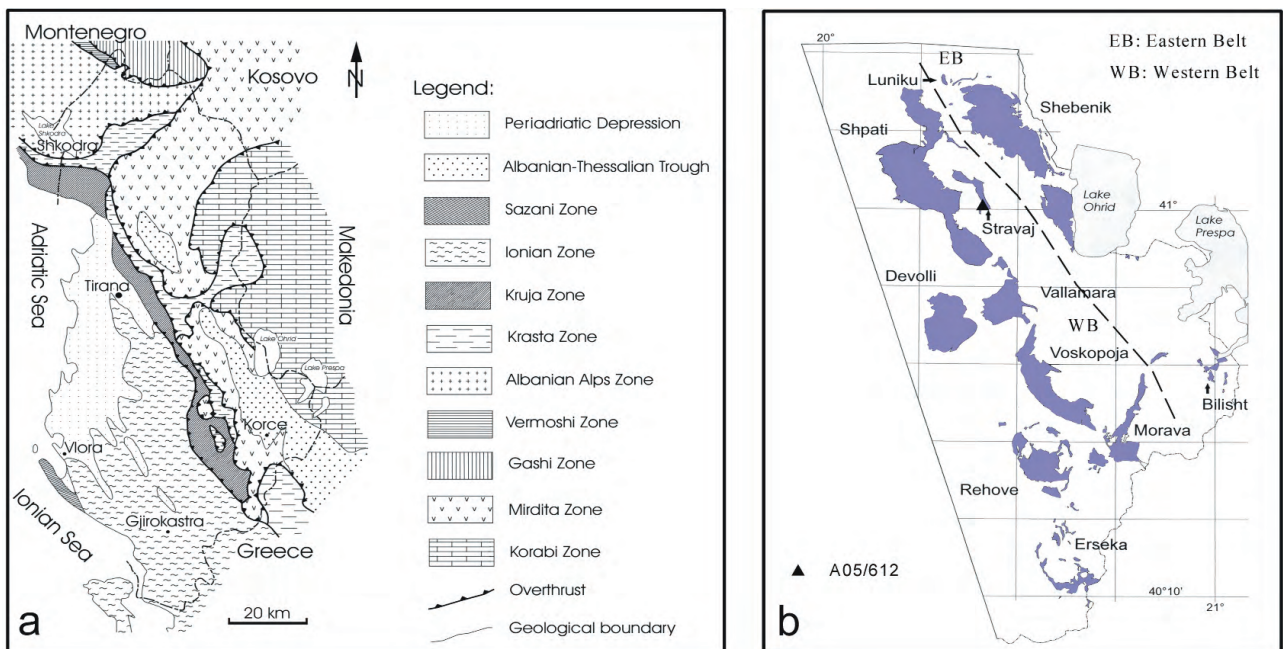
Figure 1. (a) Generalized Geology of Albania after Meco & Aliaj (2000). (b) Distribution of ophiolite massifs of southern Albania showing the sample locality within the Stravaj massif. The division into a western and an eastern belt is also shown.

the lower cumulates (Beccaluva *et al.* 1994; Bébien *et al.* 1998).

Hoeck & Koller (1999) observed for the first time that in the western ophiolite belt in southern Albania SSZ lavas also occur. Bortolotti *et al.* (2002) and Hoeck *et al.* (2002) demonstrated that the western belt also shows subduction influence. Koller *et al.* (2006) reported that in the western belt of the southern Mirdita belt significant SSZ-related magmas occur, not only within the volcanic sequences but also in the plutonic rocks.

The rocks of the eastern and western belt probably originated from the same oceanic basin as the occurrence of sedimentary cover and common metamorphic sole suggests (Bortolotti *et al.* 1996). Bébien *et al.* (2000) hypothesized that both types of ophiolites are related to an early stage of subduction, but this suggestion disagrees with the general view about the Mirdita Ophiolite Belt (Beccaluva *et al.* 1994; Shallo 1994; Bortolotti *et al.* 1996; Hoeck & Koller 1999; Dilek *et al.* 2007). The coeval presence of different magma types in the western belt is the result of mid-ocean ridge magmatism in a proto fore-arc region (Bortolotti *et al.* 1996), and the volcanic sequences of the eastern belt almost exclusively characterized by low-Ti and boninitic volcanic rocks reflecting a supra-subduction origin (Beccaluve *et al.* 1994; Bortolotti *et al.* 1996; Hoeck & Koller 1999). The predominance of the MOR-type over SSZ-type crustal rocks, together with the occurrence of volcanogenic sediments above the ophiolites, do not exclude the ophiolites originating in a back-arc basin with westward dipping subduction (Koller *et al.* 2006). An alternative interpretation places the genesis of the western ophiolites in a fore-arc basin setting above an eastward dipping subduction zone (Bortolotti *et al.* 2002; Dilek *et al.* 2007, 2008).

Ar^{40}/Ar^{39} ratios measured in hornblende from metamorphic soles and gabbros (Bébien *et al.* 2000), and palaeontological evidence (radiolaria) (Marcucci & Prela 1996) suggest that ophiolites from both belts formed during the middle–late Jurassic. The ages of the ophiolites in the western belt of the southern Mirdita belt range in age from 169 to 174 Ma (Bébien *et al.* 2000).

Part of the southern Mirdita belt is the Stravaj massif (Figure 1b) from which the mafic rock samples studied here were collected.

Stravaj is a small massif in the western part of the Mirdita belt (Hoeck *et al.* 2007). It is located east of the large Sphati massif and west of the Shebenik massif as part of the eastern SSZ belt (Figure 1b). The Stravaj massif (Figure 2) consists of basal plagioclase peridotites of lherzolitic composition, crosscut by rodingitized gabbro dykes, overlain by an isotropic gabbro cover, in turn overlain by pillow lavas. The pillow lava sequences are locally cut by basaltic dykes (Figure 2). Stravaj is one of the southern Albanian massifs, along with Voskopoja and Rehove (Hoeck *et al.* 2002), which contains a volcanic section. In this paper we studied basalt dykes taken from the upper pillow lava sequence.
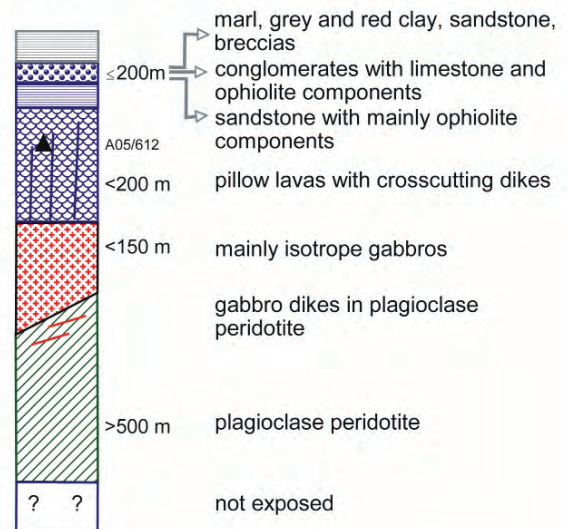
Figure 2. Schematic profile section through the Stravaj massif including the approximate position of the investigated sample.

Sample Collection

The studied basalt samples (A05/612) are from the Stravaj massif in the Mirdita Ophiolite Belt (southern Albania). A05/612 basalt is a basaltic dyke crosscutting the higher pillow sequence (pillow basalts, dykes) and possibly part of the Western belt. We studied the abundant chromian spinel in former olivine and groundmass. Spinel was picked after the basalt samples were crushed. About 100 double polished spinel grains were analyzed.

Analytical Methods

Bulk major and trace element compositions of basalt were analyzed by X-ray fluorescence (XRF) using a PHILIPS PW 2400 at the Department of Lithospheric Research, University of Vienna. For major elements a lithium-borate melt bead and for the trace elements a pressed powder pellet was used. The loss on ignition (LOI) was determined by heating in a furnace at 1000°C for three hours.

Spinel heating experiments were conducted using Carl-Zeiss-Jena HB-50 type furnace following the method of Kamenetsky (1996). The upper temperature limit of the furnace is 1660°C. The samples were heated to 1200±20°C and then to 1240±20°C, based on reference data (Kamenetsky 1996).

Compositions of the homogenized melt inclusions, unheated melt inclusion phases (clinopyroxene daughter mineral + glass phase), bulk rock, rock-forming clinopyroxene and melt inclusion host spinel were determined using an electron microprobe. Major element compositions of the analyzed phases were determined with a CAMECA SX-100 electron probe X-ray microanalyzer at the Department of Lithospheric Research, University of Vienna, Austria. During the measurements an accelerating voltage of 15 kV, beam current of 10 nA, beam size of 1–10 mm (10 mm only for investigation of silicate melt inclusions), and 40 sec of counting time were used. Standard ZAF corrections were applied.

Trace element compositions of the homogenized melt inclusions and host spinel were analyzed using LA-ICP-MS. The measurements were carried out using an ELAN-DRCe ICP-MS instrument (Perkin Elmer) equipped with a 193 nm ArF laser (Geolas) at the University of Bern, Switzerland. Laser output energy was 70 mJ/pulse, with 5–15 J/cm2/pulse flux on the sample surface. Laser frequency was 7 Hz, beam size was 24–90 mm.

Petrography

Basalt

The studied rocks normally have a porphyritic texture, and most are strongly altered (serpentinized). Former olivine phenocrysts, originally euhedral, are completely replaced by serpentine minerals (Figure 3a). Former olivine phenocrysts vary in size between 0.3 and 7.0 mm and form groups (aggregates) in the studied basalt (Figure 3a). Olivines contain numerous spinel inclusions, and spinel also occurs in the groundmass (Figure 3a). Spinels appear as opaque, fresh grains 100 to 300 μm across in both the olivine phenocrysts and the groundmass (Figure 3a, b). They are brown, octahedral, often show petrographic signs of slight magmatic resorption, and commonly have an oxidized rim of magnetite (Figure 3b). The strongly altered groundmass originally consisted of silicate glass, amphibole, clinopyroxene and plagioclase microcrysts.
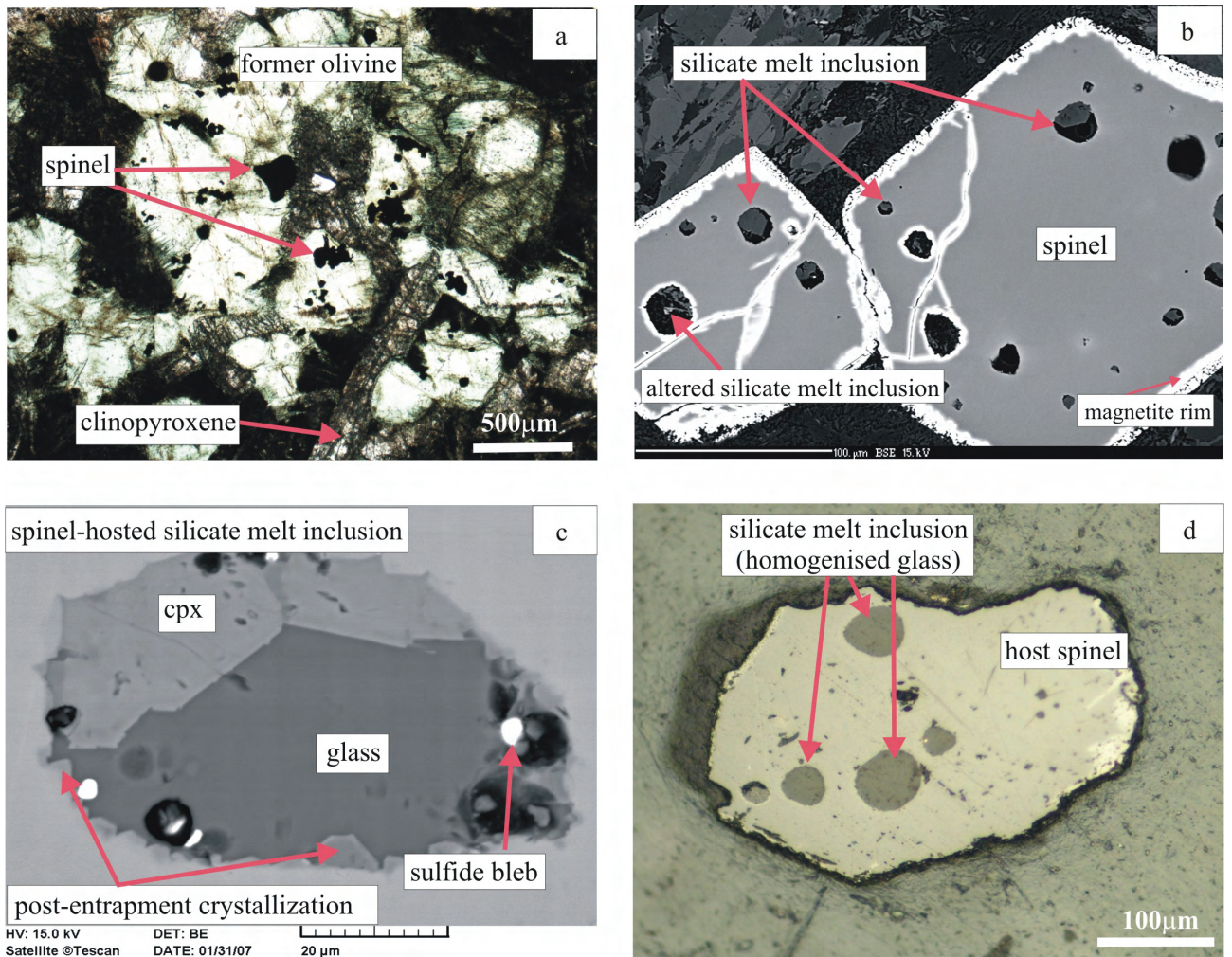
Melt Inclusions in Spinel

Spinel grains contain numerous silicate melt inclusions, which can be observed with reflected light on polished surface (Figure 3c). The inclusions, 5 to 80 μm in diameter, show primary petrographic features, are isometric and trapped randomly in the host minerals (Figure 3b, d). They show sometimes the former crystal/melt interface. Silicate melt inclusions in the studied spinels can be divided into two petrographic groups: fresh and altered silicate melt inclusions. The fresh melt inclusions are multiphase; consisting mainly of glass, clinopyroxene daughter minerals and sulphide blebs (Figure 3b, c). A small portion (2–3 μm thick in section) of spinel post-entrapment crystallization can be observed on the wall of the silicate melt inclusions (Figure 3c). Fluid entered some of the melt inclusions through cracks in the spinel. Such melt inclusions are altered, with secondary amphibole and plagioclase infill and have a magnetite bearing rim towards the host spinel (Figure 3b). These melt inclusions were not used for the heating experiments.

Geochemistry

Whole Rock Chemistry

All samples studied here are basalt from dykes, which intruded pillow basalts of the ophiolitic sequence. The bulk composition of the studied rocks is characterized by a high MgO content (up to 14 wt%), and the average mg# (Mg/Mg+Fe^{2+}) is 75.4. The SiO$_2$ content is around 46 wt%, Al$_2$O$_3$ concentration is 14 wt%, CaO content is 10.5 wt%, Na$_2$O content

Figure 3. (a) Thin section picture (+ nicols) of sample A05/612 with relics of olivine, spinel, cpx and groundmass; **(b)** BSE image of idiomorphic spinel crystals with an alteration rim of magnetite, hosting fresh and altered silicate melt inclusions; **(c)** BSE image with details of a silicate melt inclusion with post-entrapment crystallization of cpx, a glass phase, various bubbles and sulphide blebs; **(d)** BSE image of a homogenized silicate melt inclusions in a chromite grain.

is 1.7 wt% and TiO_2 content is 0.7 wt% on average. The studied basalt is characterized by FeO_{total} content (8.9 wt%) and has a fairly high concentration of compatible elements, such as Cr (706 ppm), V (151.6 ppm) and Ni (468 ppm) (Table 1).

Mineral Chemistry

Olivine phenocrysts in the studied sample are completely altered. The chromian spinels are characterized by high Cr_2O_3 and MgO contents: the estimated cr# [Cr/(Cr+Al)] is between 0.35–0.48, and

the mg# is between 0.75 and 0.78. The TiO_2 content is low: 0.24–0.27 wt% and the concentration of Al_2O_3 is up to 36.7 wt% (Figure 4, Table 2). They have high concentration of compatible elements: Ni ranges between 1509 and 2018 ppm; Co is around 200 ppm and Zn is 566–966 ppm, while V ranges between 852 and 986 ppm (Table 3).

In the groundmass the slightly altered rock-forming clinopyroxenes (cpx) show very primitive composition. Clinopyroxene phenocrysts have an enstatitic composition (En= 43.9–46.0), high Mg# (75–81), high CaO content (17.8–21.8 wt%)
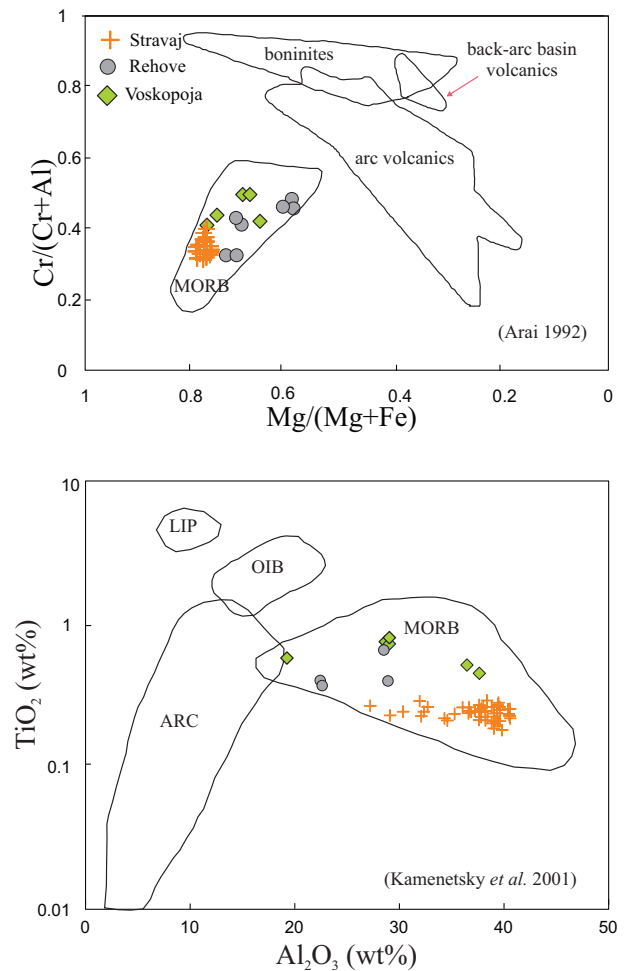
Table 1. Major and trace element composition of chromite-bearing basalts from South Albanian ophiolites (XRF data, total Fe as Fe_2O_3); n.d. not detected.

| Sample | A05/612 | A99/026 | A00/186 | Alb3/98 | A99/058 |
Massif	Stravaj	Voskopoja	Voskopoja	Rehove	Rehove
SiO_2	45.96	50.47	45.21	47.97	47.06
TiO2	0.70	1.26	0.85	0.96	0.92
Al_2O_3	14.12	15.04	14.69	16.33	15.79
Fe_2O_3	9.00	9.39	8.57	8.80	9.01
MnO	0.14	0.17	0.14	0.14	0.16
MgO	13.93	8.34	12.84	9.49	11.27
CaO	10.51	9.40	12.57	10.69	10.04
Na_2O	1.74	3.42	1.75	2.40	2.61
K_2O	0.04	0.63	0.05	0.33	0.36
P_2O_5	0.04	0.12	0.06	0.08	0.07
LOI	3.66	2.59	3.72	2.55	3.12
Total	99.84	100.83	100.45	99.74	100.41
Nb	2.5	2.0	1.9	0.3	0.8
Zr	32.7	81.70	61.4	53.7	46.9
Y	16.8	24.4	21.5	19.2	16.8
Sr	67.2	237.1	136.4.	125.3	157.6
Rb	0.7	6.4	3.4	n.d.	2.9
Ga	11.1	16.2	8.6	12.5	14.1
Zn	56.3	58.6	68.7	38.0	71.7
Cu	64.9	88.0	62.2.	54.8	93.1
Ni	467.8	131.8	406.6	169.4	326.5
Co	49.4	44.5	49.2	n.d.	48.8
Sc	14.9	31.8	21.1	34.8	25.9
Cr	706.2	338.2	700.7	339.2	580.3
V	151.6	207.1	156.4	182.9	164.3
Ba	26.5	26.8	21.9	10.4	36.8

Figure 4. Chromian spinel compositions in primitive basalts from Stravaj and from the South Albanian ophiolites (reference data for Rehove and Voskopoja according to Hoeck *et al.* 2002). **(a)** Mg/(Mg+Fe) vs Cr/(Cr+Al) with compositional fields after Arai (1992). **(b)** Al_2O_3 vs TiO_2 with compositional fields after Kamenetsky *et al.* (2001). LIP for large igneous provinces, OIB ocean island basalts, MORB middle ocean ridge basalts, ARC island arc basalts.

while Cr_2O_3 ranges up to 0.54 wt%. They have low TiO_2 (0.78–1.53 wt%), Al_2O_3 (2.89–5.24 wt%) and Na_2O (0.27–0.30) contents (Figure 5). The SiO_2 concentration ranges between 49.3–51.8 wt% (Table 4). Clinopyroxene is commonly altered to actinolite.

Spinel-hosted Silicate Melt Inclusion Chemistry

The clinopyroxene daughter minerals within the silicate melt inclusions have a more primitive composition than the rock-forming clinopyroxene phenocrysts (Figure 5). They have 49.7 wt% SiO_2 concentration on average, high Mg# (82.0), 0.69 wt% TiO_2, 8.03 wt% Al_2O_3, 16.5 wt% CaO, and high Cr_2O_3 (0.91–1.10 wt%) content (Table 5). Based on the analyses and the backscattered electron images of the clinopyroxene daughter minerals, they are unzoned (Figure 3c). The compositions of the glass in the unheated melt inclusions vary, with 57.1–64.6 wt% SiO_2, 22.5–25.8 wt% Al_2O_3, 6.30–9.68 wt% CaO,

Table 2. Fresh spinel composition for sample A05/612 from the Stravaj ophiolite complex (southern Albania) including Mg# and Cr# according to a formula calculation for 4 oxygen atoms and the calculated end members of the spinel group. Fe^{3+} calculated by (2-Al-Cr-Ti).

Spinel	109	110	111	112	113	114	435 (rim)
TiO_2	0.26	0.27	0.24	0.24	0.26	0.25	0.09
Al_2O_3	34.22	31.58	36.49	36.23	36.69	35.98	2.30
Cr_2O_3	33.72	36.99	31.70	31.51	31.29	31.86	23.64
FeO	13.61	14.01	13.40	13.30	13.35	13.75	60.74
MnO	0.12	0.18	0.13	0.12	0.09	0.17	1.99
NiO	0.20	0.24	0.24	0.26	0.26	0.27	0.06
MgO	18.33	17.67	18.59	18.60	18.77	18.65	0.51
CaO	0.03	0.01	0.02	0.02	0.00	0.00	0.00
Total	100.49	100.95	100.81	100.28	100.71	100.93	89.33
Al	1.147	1.069	1.208	1.206	1.214	1.193	0.109
Ti	0.006	0.006	0.005	0.005	0.005	0.005	0.003
Cr	0.758	0.840	0.704	0.703	0.694	0.709	0.850
Fe^{3+}	0.089	0.085	0.083	0.086	0.087	0.093	1.038
Fe^{2+}	0.235	0.251	0.231	0.228	0.227	0.231	0.900
Mn	0.003	0.004	0.003	0.003	0.002	0.004	0.067
Ni	0.004	0.005	0.005	0.006	0.006	0.006	0.002
Mg	0.777	0.756	0.778	0.783	0.785	0.782	0.031
Mg#	0.77	0.75	0.77	0.77	0.78	0.77	0.03
Cr#	0.40	0.44	0.37	0.37	0.36	0.37	0.87
Magnetite	4.45	4.25	4.16	4.30	4.33	4.64	51.68
Ulvospinel	0.28	0.29	0.26	0.25	0.27	0.26	0.15
Chromite	37.92	42.00	35.19	35.17	34.72	35.43	42.08
Pleonast	57.35	53.46	60.39	60.28	60.68	59.66	6.09

Figure 5. Cpx composition in chromite-bearing basalt on a Mg/$(Mg+Fe^{2+})$ vs Na_2O/Al_2O_3 diagram with fields for rock-forming clinopyroxenes and clinopyroxene daughter mineral of the melt inclusions.

and 3.40-6.17 wt of Na_2O. MgO is low, ranging up to 1.56 wt% (Table 5).

Homogenized silicate melt inclusions are uniform and consistently basaltic in composition, containing 48.1–51.7 wt% SiO_2. They have high concentrations of MgO (9.8–12.7 wt%, Mg#: 74.6–83.2), Al_2O_3 (14.6–17.4 wt%), FeO (5.31–7.72 wt%), CaO (12.0–13.1 wt%) and Cr_2O_3 (0.81–1.07 wt%) (Table 6). Homogenized silicate melt inclusions have 142–230 ppm V, 27–80 ppm Co, 813–122 ppm Ni, 50–390 ppm Zn content. Rare earth elements show variable distribution, La concentration ranges between 0.21–0.34 ppm, Eu, Y and Lu concentrations range between 0.28–0.71 ppm, 12.96–21.30 ppm and 0.25–0.77 ppm, respectively (Figure 6a, b and Table 7): it is more significant to report the whole REE content and the range of La/Lu, than ranges above. Average PM-normalized La_N/Lu_N ratio is 1.18–0.28.

Table 3. Representative trace element composition of spinel hosted by olivine and from the groundmass in ppm, including the relative uncertainty (1σ) of the LA-ICP-MS spinel measurement.

Spinel	III/3_02	III/23_02	III/45_02	III/50_01	III/32_02	II/16_01	1σ
Nb	0.43	0.49	0.50	0.45	0.42	0.32	0.3%
Zr	0.19	0.42	0.66	0.35	0.39	0.73	0.1%
Zn	639.50	653.21	996.22	621.74	566.65	695.88	1.3%
Cu	7.79	5.50	5.26	5.56	4.50	5.38	0.7%
Ni	1983.70	2018.65	2010.91	1756.78	1578.11	1509.99	1.6%
Co	220.99	206.61	205.18	184.26	178.21	175.43	0.6%
V	976.88	986.18	852.78	853.78	881.79	953.31	0.4%

Table 4. Representative major element composition from rock-forming clinopyroxene, EMS data in wt%, total Fe as FeO, formula calculation based on six oxygen atoms, Mg# based on $Mg/(Mg+Fe^{2+})$.

Cpx	406	407	416	417	418	419	420	421
SiO_2	50.06	50.16	51.83	49.30	49.90	50.15	50.18	49.82
TiO_2	1.31	1.18	0.78	1.53	1.13	0.93	0.92	1.46
Al_2O_3	4.28	3.95	2.89	5.01	5.24	4.85	5.00	4.99
Cr_2O_3	0.52	0.33	0.24	0.18	0.26	0.26	0.21	0.54
FeO	8.61	9.32	10.02	8.08	6.77	6.89	7.59	7.19
MnO	0.22	0.22	0.28	0.21	0.16	0.17	0.20	0.20
NiO	0.00	0.02	0.03	0.03	0.04	0.01	0.03	0.04
MgO	15.33	15.28	16.14	15.24	14.99	15.11	15.73	15.04
CaO	19.92	19.62	17.80	20.08	21.69	21.80	19.94	20.77
Na_2O	0.27	0.27	0.27	0.28	0.30	0.28	0.24	0.28
K_2O	0.02	0.01	0.00	0.00	0.00	0.00	0.00	0.00
Total	100.54	100.36	100.28	99.94	100.48	100.45	100.04	100.33
Si	1.853	1.863	1.917	1.833	1.840	1.850	1.854	1.841
Al	0.187	0.173	0.126	0.219	0.228	0.211	0.218	0.217
Ti	0.036	0.033	0.022	0.043	0.031	0.026	0.026	0.041
Cr	0.015	0.010	0.007	0.005	0.008	0.007	0.006	0.016
Fe^{2+}	0.266	0.290	0.310	0.251	0.209	0.213	0.235	0.222
Mn	0.007	0.007	0.009	0.006	0.005	0.005	0.006	0.006
Mg	0.846	0.846	0.890	0.845	0.824	0.831	0.866	0.828
Ca	0.790	0.781	0.705	0.800	0.857	0.862	0.789	0.822
Na	0.019	0.019	0.019	0.020	0.021	0.020	0.017	0.020
Total	4.019	4.022	4.005	4.022	4.023	4.025	4.017	4.013
Mg#	0.76	0.75	0.74	0.77	0.80	0.80	0.79	0.79

Discussion

Estimation of Crystallization Conditions of the Basaltic Dikes

The composition of the homogenized silicate melt inclusions significantly differs from the composition of the bulk rock (Tables 1 & 5): the most evident difference is in their MgO-content. Graphic projection of the compositions in the diopside-anorthite-forsterite ternary diagram (studied by Presnall *et al.* 1978, basalt phase diagram at 0.7 GPa) demonstrate the chemical diversity of the homogenised silicate melt inclusions and the bulk rock (Figure 7). The composition of the basaltic bulk rock falls within the stability field of olivine, however the composition of silicate melt inclusions lies on the clinopyroxene-spinel cotectic line. The texture of the studied rock is characterised by olivine aggregates, while the spinel crystals are present in the groundmass or in the olivines as crystal inclusions (Figure 3a). This textural feature can be interpreted as the result of the following crystallization path of the magma: the first crystallizing phase is olivine, followed by the simultaneous crystallization of spinel and olivine when the composition of the crystallizing melt reaches the spinel-olivine cotectic line with decreasing temperature (Figure 7). As a consequence, the bulk rock compositions measured in the samples are that of an olivine-bearing crystal-cumulate, and do not represent the bulk composition of the parent melt.

Table 5. Pairs of cpx and glass phase micro-analytical data from various silicate melt inclusions in sample A05/612, EMS data in wt%, total Fe as FeO, formula calculation for Cpx based on six oxygen atoms, Mg# based on $Mg/(Mg+Fe^{2+})$, for the glass phase a formula calculated with eight (plagioclase) oxygen atoms.

	1. pair		2. pair		3. pair	
	cpx	glass	cpx	glass	cpx	glass
Sample	396	399	402	404	450	451
SiO_2	48.55	57.14	49.48	60.91	49.03	64.68
TiO_2	0.89	0.20	0.86	0.35	0.73	0.46
Al_2O_3	9.03	25.89	7.59	25.28	8.74	22.50
Cr_2O_3	1.10	0.65	0.97	0.60	0.91	0.58
FeO	5.66	0.75	5.46	0.54	5.83	0.53
MnO	0.15	0.00	0.12	0.01	0.15	0.02
NiO	0.00	0.05	0.01	0.08	0.02	0.01
MgO	16.23	1.56	17.98	0.19	17.30	0.32
CaO	18.58	9.68	18.38	7.66	17.54	6.30
Na_2O	0.23	4.71	0.14	6.17	0.22	3.40
K_2O	0.00	0.04	0.00	0.00	0.00	0.02
Total	100.42	100.67	100.99	101.79	100.47	98.82
Si	1.767	2.603	1.787	2.690	1.778	2.880
Al	0.387	1.390	0.323	1.316	0.373	1.181
Ti	0.024		0.023		0.020	
Cr	0.032		0.028		0.026	
Fe^{2+}	0.172	0.029	0.165	0.020	0.177	0.020
Mn	0.005		0.004		0.005	
Mg	0.880		0.968		0.935	
Ca	0.724	0.472	0.711	0.362	0.681	0.301
Na	0.016	0.416	0.010	0.528	0.015	0.294
K	0.000	0.002	0.000	0.000	0.000	0.001
Mg#	0.837		0.854		0.841	

Interestingly, the composition of the homogenized silicate melt inclusions lie on the clinopyroxene-spinel cotectic line, not on the spinel-olivine cotectic line. In the homogenized silicate melt inclusions, geochemical signs of a grain boundary-layer effect (Webster & Rebbert 2001) can be identified. Based on the major mineral chemistry and trace element composition of the reheated inclusions, the crystallizing melt was depleted in components incorporated in spinel and olivine around the precipitated spinel and olivine crystals. Thus, the composition of the homogenised silicate melt inclusions does not fully represent the composition of the primitive parent magma because of this grain boundary-layer effect (Webster & Rebbert 2001), although it may still provide one of the best available tools to study near-primitive magma composition and evaluation.

Estimation of Olivine Composition – Mg/Fe^{2+} partitioning between olivine and coexisting melt is mostly controlled by temperature (Ford *et al.* 1983). Olivine phenocrysts in the studied samples are completely altered, so no compositional data can be acquired from them. Spinel crystals exist as inclusions in altered olivine, therefore an equilibrium state can be assumed between them. If so, then the basic rules of geochemistry dictate that spinel-hosted silicate melt inclusions and olivine crystals are also in equilibrium with each other. Based on

Table 6. Major element composition of homogenized silicate melt inclusions in Sample A05/612; all data by EMS in wt%, total Fe as FeO, CIPW Norm calculation (Mg# based on Mg/(Mg+Fe^{2+})).

Sample	01_01	02_01	05_01	05_02	05_03	07_01	10_01	10_02	10_03	11a_01
SiO$_2$	50.73	51.48	51.04	50.63	50.71	50.83	49.50	49.38	48.10	51.70
TiO$_2$	0.78	0.67	0.73	0.72	0.68	0.78	0.88	0.74	0.79	0.73
Al$_2$O$_3$	16.51	16.07	16.10	15.74	16.88	14.63	17.20	17.40	16.35	16.21
Cr$_2$O$_3$	0.83	0.91	0.91	0.93	0.87	0.81	0.89	0.87	1.07	1.00
FeO	5.64	5.53	5.99	5.38	5.31	6.80	5.71	6.35	7.52	5.72
MnO	0.10	0.13	0.13	0.12	0.10	0.13	0.09	0.09	0.12	0.13
NiO	0.01	0.00	0.01	0.00	0.03	0.00	0.00	0.00	0.02	0.04
MgO	11.21	11.15	11.18	12.69	11.32	12.36	10.26	9.87	10.52	10.71
CaO	12.32	12.10	12.54	12.36	12.77	12.03	13.06	12.75	12.45	12.45
Na$_2$O	2.37	2.38	2.18	2.03	2.29	1.99	2.19	2.01	2.41	2.39
K$_2$O	0.01	0.00	0.00	0.00	0.08	0.00	0.00	0.00	0.01	0.01
P$_2$O$_5$	0.05	0.02	0.02	0.06	0.05	0.04	0.01	0.00	0.01	0.05
Total	100.56	100.44	100.83	100.66	101.09	100.40	99.79	99.46	99.37	101.14
Magnetite	1.39	1.36	1.47	1.32	1.30	1.68	1.42	1.58	1.88	1.40
Ilmenite	1.48	1.28	1.39	1.37	1.28	1.49	1.68	1.42	1.52	1.38
Apatite	0.12	0.06	0.04	0.15	0.13	0.10	0.02	0.00	0.03	0.12
Orthoclase	0.07	0.00	0.00	0.00	0.38	0.00	0.00	0.00	0.06	0.07
Albite	20.08	20.18	18.46	17.22	19.36	16.95	18.75	17.26	20.73	20.20
Anortite	34.49	33.34	34.18	33.87	35.53	31.13	37.51	38.97	34.29	33.39
Diopside	19.76	19.97	20.86	20.19	20.41	21.35	20.88	18.81	21.27	20.84
Hypersthene	13.34	17.69	16.74	16.32	11.00	20.20	9.91	14.68	2.11	17.00
Olivine	8.07	4.77	5.50	8.18	9.33	5.91	8.51	5.98	16.52	4.12
Mg#	80.72	80.93	79.69	83.23	81.76	79.26	79.09	76.57	74.63	79.75
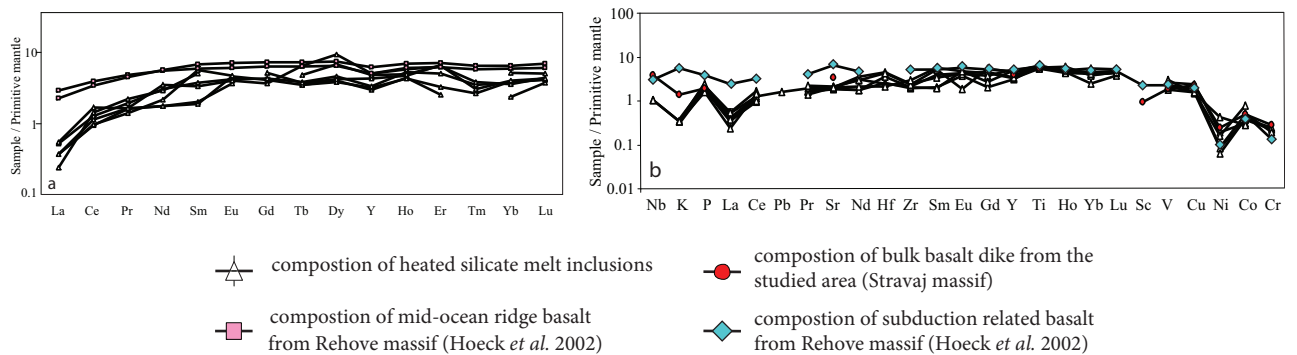
Figure 6. (a) REE distribution patterns of six homogenized silicate melt inclusions in Stravaj and related MORB samples (according to Hoeck *et al.* 2002); normalizing values according to Sun & McDonough (1989). **(b)** Trace element concentrations for homogenized silicate melt inclusions, host basalt rock (A05/612) and reference basalts from Rehove (Hoeck *et al.* 2020); normalizing values according to Sun & McDonough (1989).

Table 7. Trace element compositions of the homogenized silicate melt inclusions. All data in ppm, all values by LA-ICP-MS including the relative uncertainty (1σ) of the LA-ICP-MS.

ppm	III/3	III/23	III/45	1σ
				%
Nb	<0.08	<0.12	<0.04	0.30
Zr	20.60	21.15	21.84	0.10
Y	12.96	13.91	14.47	0.30
Sr	38.78	35.75	40.63	0.40
Rb	<0.07	<0.16	0.12	0.60
Zn	50.73	55.23	60.95	1.30
Cu	46.43	113.13	370.32	0.70
Ni	160.02	122.59	230.78	1.60
Co	37.38	39.67	51.29	0.60
V	142.27	164.40	154.47	0.40
Ba	<0.25	<0.70	<0.10	0.80
Mo	<0.33	<0.40	<0.29	0.50
Cs	<0.02	<0.03	<0.01	0.80
Pb	<0.20	<0.26	0.24	0.10
Th	<0.04	<0.06	<0.01	0.10
U	<0.04	<0.07	<0.03	0.10
La	0.24	0.24	0.34	0.30
Ce	1.92	1.58	2.14	0.40
Pr	0.42	0.41	0.49	0.10
Nd	2.18	2.21	3.80	0.40
Sm	0.83	0.77	1.53	0.10
Eu	0.57	0.71	0.66	0.60
Gd	1.12	2.25	2.37	0.40
Tb	0.35	0.35	0.38	0.20
Dy	2.59	2.50	3.02	0.10
Ho	0.65	0.64	0.79	0.60
Er	1.11	1.45	2.22	0.20
Tm	0.28	0.18	0.24	0.20
Yb	1.06	1.74	1.67	0.30
Lu	0.25	0.28	0.28	0.50
Hf	0.71	1.00	0.69	0.20
Ta	<0.01	<0.03	<0.01	0.30
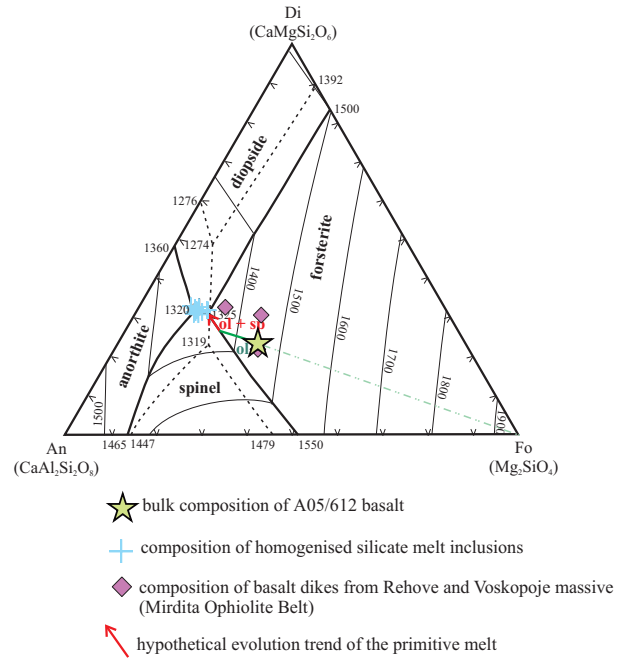
Figure 7. An-Di-Fo phase diagram after Presnall *et al.* (1978) (solid line at 7 kbar, dashed line at 1 atm) with the bulk composition of sample A05/612, the composition of homogenized silicate melt inclusions and a hypothetical evolution trend and reference basalts from Rehove and Voskopoja (Hoeck *et al.* 2002).

this assumption, we used Ford's equation (Ford *et al.* 1983) to calculate the forsterite content of olivine, which could have coexisted with spinel and mafic melt trapped as spinel-hosted silicate melt inclusion. Accordingly, the calculated forsterite content of altered olivines in our samples ranges from 86 to 90 mol%.

Forsterite content of olivine can also be estimated based on the Cr# and Mg# of spinels coexisting with olivine at a given temperature (Kamenetsky *et al.* 2001). Kamenetsky's method is based on empirical observations carried out at 1100±71°C. Based on the results of our homogenization experiments on the silicate melt inclusions, this temperature is a good approximation of the crystallization temperature of the cogenetic olivine and spinel phases. According to this assumption, the forsterite content of olivine that would have been in equilibrium with the studied spinels is 88–90% at 1100±71°C.

These estimates agree well with the forsterite content of olivine calculated using the method of Ford *et al.* (1983), and is also similar to measured compositions of olivines from gabbros in the nearby Voskopoja, Morava, Sphati, Rehove, Devolli and Vallamara massifs (Fo 84–89%) (Koller *et al.* 2006).

Pressure – The crystallization pressure was estimated using the geobarometric method of Nimis & Ulmer (1998) for magmatic systems. It is calibrated for anhydrous basaltic melt systems and is temperature independent (standard error: ±1.7 kbar). We used the composition of rock-forming clinopyroxenes (Table 4) for the calculations, based on a range of 1.81 to 2.86±1.7 kbar, to estimate crystallization pressures. This pressure range is characteristic of late stage episodes of magma evolution.

Koller *et al.* (2006) estimated a similar crystallization pressure range (2.1–3.8±1.7 kbar) for gabbros from the Voskopoje, Rehove, Luniku and Sphati massifs (Mirdita ophiolite Belt) using the method of Nimis & Ulmer (1998).

Temperature – The crystallization temperature of the host spinel was determined using homogenization experiments on the silicate melt inclusions. The homogenization temperature value (with the absence of daughter minerals) of the silicate melt inclusions at 1240±20°C, is the minimum trapping temperature of the inclusions (Roedder 1984) and indicates the minimum crystallization temperature of the host spinel.

Oxygen Fugacity – Spinels in basaltic rocks generally provide well-based information about the redox state of the source region of basalt, because they are resistant to major alteration during crystallization (Ballhaus *et al.* 1991). Oxygen fugacity was estimated from equilibrium compositions of olivine-spinel using the method of Ballhaus and co-workers (1991). Olivine composition was calculated based on the method of Ford *et al.* (1983). Values of $\log(fO_2)$ range from –0.64 to 0.14, with an average of –0.22 at a temperature of 1240°C. The values range around the QFM (quartz-fayalite-magnetite) buffer, and estimated oxygen fugacity data correspond well with

the $\log fO_2$ values typical of MOR basalts (FMQ-2 to FMQ0) (Ballhaus *et al.* 1991) (Figure 8).
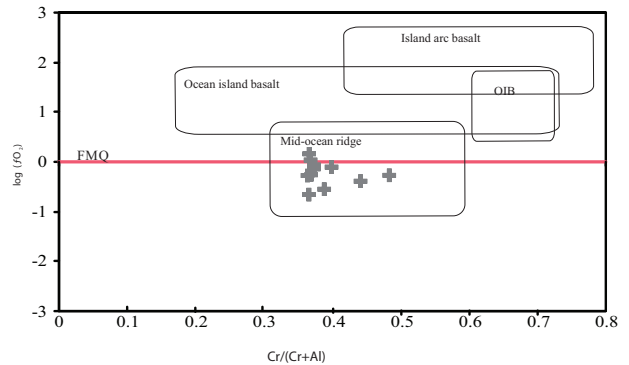
Figure 8. Chromite plot Cr/(Cr+Al) vs. delta log fO_2 according to Ballhaus *et al.* (1991) including fields for island arc basalt, ocean island basalts and cumulates and mid-ocean ridge basalt.

Spinel-Melt Partition Coefficient Values – Spinels are one of the earliest crystallizing phases and are predominant in mafic magmas, with special respect to primitive MORB or OIB. Many previous studies showed that the composition of spinels is a function of magma composition (Irvine 1965, 1967; Dick & Bullenb 1984; Allan *et al.* 1988; Arai 1992; Kamenetsky *et al.* 2001), temperature, and oxygen fugacity (Ballhaus *et al.* 1991). The spinel-hosted silicate melt inclusions have rarely been studied previously (Kamenetsky 1996; Lenaz *et al.* 2000; Kamenetsky *et al.* 2001) because spinels are usually opaque phases and their silicate melt inclusions remain invisible with optical microscopy. Previous studies on the partitioning coefficient of major and trace elements between spinel and coexisting melt are experimentally based using synthetic or natural melts doped with Cr, V, Co and Ni (Leeman 1974; Leeman & Lindstrom 1978; Nielsen *et al.* 1994; O'Neill & Eggins 2002; Satari *et al.* 2002; O'Neill & Berry 2006; Righter *et al.* 2006) or using groundmass glass of basaltic rocks as a substitute model for cotectic glass (Li *et al.* 2008).

Spinels are known to concentrate transitional metals, such as V, Co, Ni and Cr. Recent studies on synthesised or doped natural sample systems have shown that partitioning coefficients (K_D) of Co and

Ni between spinel and coexisting melt are relatively independent of the temperature and oxygen fugacity, although a function of Co, Ni concentration in spinel. In comparison K_D of V is strongly sensitive to temperature and oxygen fugacity, as well as the V and Ti content of spinel (Righter *et al.* 2006). We have determined K_D values for representative elements from natural samples at given parameters (1240±20°C and log (fO_2) –0.64 to 0.14, FMQ) and compared them with similar values estimated from natural glass samples (Li *et al.* 2008) and experimentally doped synthetic materials (Righter *et al.* 2006) (Figure 9, Table 8). Table 8 shows K_D values of spinels and homogenised silicate melt inclusions. Based on these values transitional elements such as V, Co, Cr and Ni are extremely compatible, Al, and Mg are slightly compatible, whereas Na, Ca, Ti and Zn are incompatible to the spinel phase. K_D values determined for Ni are somewhat higher than the previously reported experimental data, although the partitioning coefficient values for Co and V are consistent with those (Figure 9). This agreement supports that spinel-hosted silicate melt inclusions provide useful information for the calculation of V, Ni and Co partitioning coefficients.
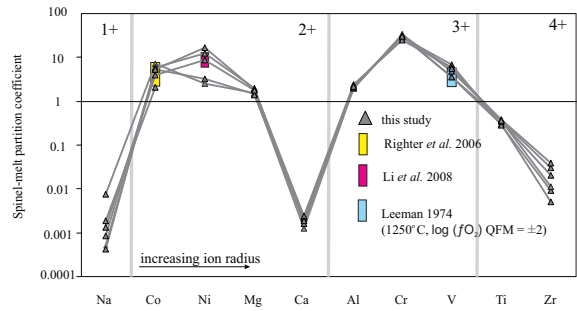
Figure 9. Calculated partition coefficient between spinel/silicate melt (homogenized silicate melt inclusions) based on increasing ion radius together with literature data based on Leeman (1974), Righter *et al.* (2006) and Li *et al.* (2008).

Melt Evolution after the Silicate Melt Inclusions were Trapped

With the gradual cooling of the magmatic system, including the trapped silicate melt inclusions, spinel phases crystallized at the edges of the inclusions (Figure 3c). This post-entrapment crystallization (PEC) changed the volume and composition of the trapped silicate drops. This phenomenon has been identified from samples with a wide range of

Table 8. Spinel/(homogenized silicate melt inclusion)-partition coefficient values at 1240±20°C and log(fO_2) between –0.64 and 0.14 (FMQ), based on EMS and LA-ICP-MS data. Vanadium data of Leeman (1974) were carried out at 1250°C and a log $f(O_2)$ 0±2 (FMQ).

K_D	1. pair	2. pair	3. pair	4. pair	5. pair	6. pair	Li *et al.* (2008) max	Li *et al.* (2008) min	Righter *et al.* (2002) max	Righter *et al.* (2002) min	Leeman (1974) max	Leeman (1974) min
Na	0.001	0.008	0.002	0.000	0.001	0.001						
Co	5.77	7.05	2.03	5.91	5.21	4.00			6	2.3		
Ni	3.28	2.51	-	12.40	16.47	8.74	11.2	6.4	9.4	6.3		
Mg	1.48	1.55	1.42	1.99	1.87	1.83						
Ca	0.002	0.001	0.002	0.002	0.002	0.002						
Al	1.96	1.94	2.08	2.17	2.40	2.20						
Cr	33.56	31.96	30.54	29.57	24.95	30.66						
V	4.48	3.44	4.50	6.87	6.00	5.52					4.3	2.3
Ti	0.37	0.36	0.30	0.29	0.35	0.36						
Zr	0.040	0.011	0.005	0.009	0.020	0.030						
Nb	-	1.21	1.36	5.43	4.05	11.58						

geological contexts (Watson 1976; Frezzotti 2001; Danyushevsky *et al.* 2002; Kress & Ghiorso 2004; Guzmics *et al.* 2008). Kamenetsky (1996) suggested that spinel-hosted melt inclusions do not suffer significant PEC due to low Cr content in the trapped melt. Based on the petrographic features of our studied inclusions, signs of PEC can be observed. Calculations based on the MELTS model (Ghiorso & Sack 1991) show up to 3% PEC in the silicate melt inclusions, assuming log$f$O$_2$= –0.22 fugacity and 5 kbar pressure and using the composition of the heated homogenised glass.

Determination of the Source Region of the Basaltic Magma

Calculations Using Spinel Composition – Spinels are excellent petrogenetic indicators in basaltic rocks, because their composition is a complex but well-studied function of the physico-chemical parameters of the source region. Cr# and Mg# of the studied spinels suggest their crystallization took place in a mid-ocean ridge region (Arai 1992) (Figure 4a). Al$_2$O$_3$ and TiO$_2$ contents of the spinel and coexisting melt show positive correlation to each other, which suggests that an Al$_2$O$_3$–TiO$_2$ discrimination diagram may be used to determine the geodynamical setting of the spinel source region (Kamenetsky *et al.* 2001) (Figure 4b). Based on the discrimination diagram, the studied spinels crystallized from MORB, and are more primitive than spinels in basalt dykes from Voskopoja and Rehove.

Calculations Based on Silicate Melt Inclusion Compositions – In the studied samples, silicate melt inclusions provide useful information about the primitive melt, because the host spinels are among the first phases to crystallize in this magmatic system (Presnall *et al.* 1978).

High Mg# of the homogenous glass suggests a primitive melt character. Basaltic magmas with high MgO contents (≥6% MgO) are often generated in mid-ocean ridges and arc-related regions. Primary arc-related magmas may have high MgO content (>6% MgO) and similar major element compositions to MOR basalts (Perfit *et al.* 1980). In the Mirdita Ophiolite Belt these two types of basalt can be found together in the ophiolite sections (Hoeck *et al.* 2002),

where they are often indistinguishable from each other in terms of petrography and major element composition, but have distinct trace element features.

Primitive mantle normalized rare earth element (REE) distribution in the homogenized silicate melt inclusions shows a strong depletion in light REE compared to the heavy REE (C1 chondrite!). The magnitude of this depletion in light REE (Figure 6a) is larger than the typical rate of depletion in basalt dykes from the Rehove massif with normal MORB composition (Hoeck *et al.* 2002). Based on the REE pattern of the silicate melt inclusions, the studied magma was not affected by subduction-related components, otherwise the light REE elements would show characteristic enrichment (Hoeck *et al.* 2002, 2007). Distribution of the middle and heavy REE is flat, which suggests an extremely depleted source region and/or a high degree of partial melting.

Multi-element spider diagrams, normalized to primitive mantle, show a similar flat pattern for middle and heavy REE content (Figure 6b), although compatible element contents (Ni, Cr) form a negative anomaly on the normalized diagram. Ni and Cr are compatible to the early crystallising spinel and olivine phases, so the melt droplets trapped in spinels are depleted in these elements. Multi-element distributions of the studied melt inclusions show a slight depletion in incompatible elements (K, La, Ce, Sr, Zr) and comparable to that of basalt dykes enriched in subduction-related components (Rehove massif in Mirdita Ophiolite Belt) (Figure 6b).

The trace element chemistry of the studied homogenised silicate melt inclusions also indicates a mid-ocean ridge origin, without the influence of subduction-related components.

Conclusions

Spinel-hosted primary, multiphase (post-entrapment crystallized spinel, clinopyroxene daughter mineral, silicate glass, occasionally sulphide blebs) silicate melt inclusions exist in basalt dykes from Stravaj massif, Mirdita Ophiolite Belt. The homogenization temperature of these silicate melt inclusion is 1240±20°C, based on homogenization experiments. This temperature range indicates the minimum crystallization temperature of the host spinel on FMQ –0.64 and +0.14 calculated oxygen fugacity

values, which are characteristic for MOR basalts. Homogenized silicate melt inclusions show a very primitive basalt composition with high Mg# (0.81). Based on the trace element distribution, the spinel-hosted magma drops represent a magma strongly depleted in light REE (La, Ce, Pr) and incompatible elements (Nb, K, Pb, Sr, Zr). The trace element distributions show obvious depletion compared to N-MORB composition, which suggest the studied basalt dykes originated at a mid-ocean ridge.

From the trace element compositions measured, distribution coefficients of Na, Co, Ni, Mg, Ca, Al, Cr, V, Ti and Zr between silicate melt and spinel have been calculated. The values obtained are consistent with experimental data from previous studies for Co, Ni and V.

Based on the petrogenetic interpretation and the texture of the studied basalt the spinel and olivine crystallized simultaneously, although a chemical boundary layer of olivine affected the major element composition and Ni content of the silicate melt inclusions.

References

ALLAN, J.F., SACK, R. & BATIZA, R. 1988. Cr-rich spinels as petrogenetic indicators: MORB-type lavas from the Lamont seamount chain, eastern Pacific. *American Mineralogist* **73**, 741–753.

ARAI, S. 1992. Chemistry of chromian spinel in volcanic rocks as a potential guide to magma chemistry. *Mineralogical Magazine* **56**, 173–184.

BALLHAUS, C., BERRY, R.F. & GREEN, D.H. 1991. High pressure experimental calibration of the olivine-orthopyroxene-spinel oxygen geobarometer: implications for the oxidation state of the upper mantle. *Contributions to Mineralogy and Petrology* **107**, 27–40.

BARNES, S.J. 2000. Chromite in komatiites II. Modification during greenschist to mid-amphibolite facies metamorphism. *Journal of Petrology* **41**, 387–409.

BARNES, S.J. & ROEDER, P. 2001. The range of spinel compositions in terrestrial mafic and ultramafic rocks. *Journal of Petrology* **42**, 2279–2302.

BECCALUVA, L., COLTORTI, M., PREMTI, I., SACCANI, E., SIENA, F. & ZEDA, O. 1994. Mid-ocean ridge and suprasubduction affinities in the ophiolitic belts of Albania. *Ofioliti* **19**, 77–96.

BÉBIEN, J., SHALLO, M., MANIKA, K. & GEGA, D. 1998. The Shebenik massif (Albania): a link between MOR- and SSZ-type ophiolites? *Ofioliti* **23**, 7–15.

BÉBIEN, J., DIMO-LAHITE, A., VERGÉLY, P., INSERGUEIX-FILIPPI, D. & DUPEYRAT, L. 2000. Albanian ophiolites I– Magmatic and metamorphic processes associated with the initiation of a subduction. *Ofioliti* **25**, 39–45.

BORTOLOTTI, V., KODRA, A., MARRONI, M., MUSTAFA, F., PANDOLFI, L., PRINCIPI, G. & SACCANI, E. 1996. Geology and petrology of ophiolitic sequences in the Mirdita region (northern Albania). *Ofioliti* **21**, 3–20.

BORTOLOTTI, V., MARRONI, M., PANDOLFI, L., PRINCIPI, G. & SACCANI, E. 2002. Interaction between mid-ocean ridge and subduction magmatism in Albanian ophiolites. *Journal of Geology* **110**, 561–576.

CORTESOGNO, L., GAGGERO, L., JAHO, E., MARRONI, M., PANDOLFI, L. & SHTJEFANAKU, D. 1998. The gabbroic complex of the western ophiolitic belt, northern Albania: an example of multilayered sequence in an intermediate-spreading ocean ridge. *Ofioliti* **23**, 49–64.

DANYUSHEVSKY, L.V., DELLA-PASQUA, F.N. & SOKOLOV, S. 2000. Re-equilibration of melt inclusions trapped by magnesian olivine phenocrysts from subduction-related magmas: petrological implications. *Contribution to Mineralogy and Petrology* **138**, 68–83.

DANYUSHEVSKY, L.V., MCNEILL, A.W. & SOBOLEV, A.V. 2002. Experimental and petrological studies of melt inclusions in phenocrysts from mantle-derived magmas: an overview of techniques, advantages and complications. *Chemical Geology* **183**, 5–24.

DICK, H.J.B. & BULLEN, T. 1984. Chromium spinel as petrogenetic indicator in abyssal and alpine-type peridotites, and spatially associated lavas. *Contributions to Mineralogy and Petrology* **86**, 54–76.

DILEK, Y., FURNES, H. & SHALLO, M. 2007. Suprasubduction zone ophiolite formation along periphery of Mesozoic Gondwana. *Gondwana Research* **11**, 453–475.

DILEK, Y., FURNES, H. & SHALLO, M. 2008. Geochemistry of the Jurassic Mirdita Ophiolite (Albania) and the MORB to SSZ evolution of a marginal basin oceanic crust. *Lithos* **100**, 174–209.

DILEK, Y., SHALLO, M. & FURNES, H. 2005. Rift-drift, seafloor spreading, and subduction tectonics of Albanian ophiolites. *International Geology Review* **47**, 147–176.

FORD, C.E., RUSSEL, D.G., CRAVEN, J.A. & FISK, M.R. 1983. Olivine-liquid equilibria: temperature, pressure and composition dependence of the crystal/ liquid cation partition coefficients for Mg, Fe²⁺, Ca and Mn. *Journal of Petrology* **24**, 256–265.

FREZZOTTI, M.L. 2001. Silicate-melt inclusions in magmatic rocks: application to petrology. *Lithos* **55**, 273–299.

GHIORSO, M.S. & SACK, R.O. 1991. Fe-Ti oxide geothermometry, geodynamic formulations and the estimation of intensive variables in silicic magmas. *Contribution to Mineralogy and Petrology* **108**, 485–510.

GUZMICS, T., ZAJACZ, Z., KODOLÁNYI, J., HALTER, W. & SZABÓ, Cs. 2008. LA-ICP-MS study of apatite- and K-feldspar-hosted primary carbonatite melt inclusions in clinopyroxenite xenoliths from lamprophyres, Hungary: implications for significance of carbonatite melts in the Earth's mantle. *Geochimica et Cosmochimica Acta* **72**, 1864–1886.

HOECK, V. & KOLLER, F. 1999. The Albanian ophiolites and the Dinaride-Hellenide framework. *EUG 10 Strasbourg, Journal of Conference Abstract* **4**, p. 406.

HOECK, V., KOLLER, F., MEISEL, T., ONUZI, K. & KNERINGER, E. 2002. The Jurassic South Albanian ophiolites: MOR- vs SSZ-type ophioltes. *Lithos* **65**, 143–164.

HOECK, V., KOLLER, F., ONUZI, K., KLOETZLI-CHOVANETZ, E. & IONESCU, C. 2007. Transition from SSZ to MORB composition in Albanian Ophiolites: evidence from small ophiolites intermediate between the eastern and the western belt (Albania). *Geophysical Research Abstracts* **9**, 1607–7962.

IRVINE, T.N. 1965. Chromian spinel as a petrogenetic indicator – Part 1: Theory. *Canadian Journal of Earth Sciences* **2**, 648–671.

IRVINE, T.N. 1967. Chromian spinel as a petrogenetic indicator – Part 2: Petrologic applications. *Canadian Journal of Earth Sciences* **4**, 71–103.

IYER, K., AUSTRHEIM, H., JOHN, T. & JAMTVEIT, B. 2008. Serpentinization of the oceanic lithosphere and some gochemical consequences: constraints from Leka Ophiolite Complex, Norway. *Chemical Geology* **249**, 66–90.

ISPGJ-FGJM-IGJN 1983. *Harta gjeologjike e Shqiperise. Scale 1: 200 000*. Tirana [in Albanian].

KAMENETSKY, V.S. 1996. Methodology for the study of melt inclusions in Cr-spinel, and implications for parental melts of MORB from FAMOUS area. *Earth and Planetary Science Letters* **142**, 479–486.

KAMENETSKY, V.S., CRAWFORD, A.J. & MEFFRE, S. 2001. Factors controlling chemistry of magmatic spinel: an empirical study of associated olivine, Cr-spinel and melt inclusions from primitive rocks. *Journal of Petrology* **42**, 655–671.

KOLLER, F., HOECK, V., MEISEL, T., IONESCU, C., ONUZI, K. & GHEGA, D. 2006. Cumulates and gabbros in southern Albanian ophiolites: their bearing on regional tectonic setting. *In*: ROBERTSON, A.H.F. & MOUNTRAKIS, D. (eds), *Tectonic Development of the Eastern Mediterranean Region*. Geological Society, London, Special Publications **260**, 267–299.

KÓTHAY, K., SZABÓ, Cs., TÖRÖK, K. & SHARYGIN, V. 2005. Egy csepp a magmából: szilikátolvadék-zárványok a hegyestűi alkáli bazalt olivin fenokristályaiban. *Földtani Közlöny* **135**, 31–57 [in Hungarian with English abstract].

KRESS, V.C. & GHIORSO, M.S. 2004. Thermodynamic modeling of post-entrapment crystallization in igneous phases. *Journal of Volcanology and Geothermal Research* **137**, 247–260.

LEEMAN, W.P. 1974. *Experimental Determination of the Partitioning of Divalent Cations Between Olivine and Basaltic Liquid*: *Pt. II*. PhD Thesis, University of Oregon, 231–337.

LEEMAN, W.P. & LINDSTROM, D.J. 1978. Partitioning of Ni²⁺ between basaltic and synthetic melts and olivine– an experimental study. *Geochimica et Cosmochimica Acta* **42**, 400–412.

LENAZ, D., KAMENETSKY, V.S., CRAWFORD, A.J. & PRINCIVALLE, F. 2000. Melt inclusions in detrital spinel from the SE Alps (Italy-Slovenia): a new approach to provenance studies of sedimentary basins. *Contribution to Mineralogy and Petrology* **139**, 748–758.

LI, C., RIPLEY, E.M., TAO, Y. & MATHEZ, E.A. 2008. Cr-spinel/olivine and Cr-spinel/liquid nickel partition coefficients from natural samples. *Geochimica et Cosmochimica Acta* **72**, 1678–1684.

LOWENSTERN, J.B. 1995. Applications of silicate-melt inclusions to the study of magmatic volatiles. Magmas, fluids, ore deposits. *In*: THOMPSON, J.F.H. (ed), *MAC Short Course* **23**, 71–100 Victoria, British Columbia.

MECO, S. & ALIAJ, S. 2000. *Geology of Albania*. Beiträge zur regionalen Geologie der Erde **28**, Gebrüder Borntraeger, Berlin, Stuttgart.

MARCUCCI, M. & PRELA, M. 1996. The Lumizi (Puke) section of the Kalur Cherts: radiolarian assemblages and composition with other sections in northern Albania. *Ofioliti* **21**, 71–76.

MEVEL, C. 2003. Serpentinization of abyssal peridotites at mid-ocean ridges. *Comptes Rendus Geoscience* **335**, 825–852.

NIELSEN, R.L., FORSYTHE, L.M., GALLAHAN, W.E. & FISK, M.R. 1994. Major- and trace-element magnetite-melt equilibria. *Chemical Geology* **117**, 167–191.

NIELSEN, R.L., CRUM, J., BOURGEOIS, R., HASCALL, K., FORSYTHE, L.M., FISK, M.R. & CHRISTIE, D.M. 1995. Melt inclusions in high-an plagioclase from the Gorda Ridge – an example of the local diversity of MORB parent magmas. *Contributions to Mineralogy and Petrology* **122**, 34–50.

NIMIS, P. & ULMER, P. 1998. Clinopyroxene geobarometry of magmatic rocks – Part 1: an expanded structural geobarometer for anhydrous and hydrous, basic and ultrabasic systems. *Contributions to Mineralogy and Petrology* **135**, 62–74.

Norman, M.D., Garcia, M.O., Kamenetsky, V.S. & Nielsen, R.L. 2002. Olivine-hosted melt inclusions in Hawaiian picrites: equilibration, melting, and plume source characteristics. *Chemical Geology* **183**, 143–168.

O'neill, H.C. & Eggins, S.M. 2002. An experimental investigation of the effect of melt composition on the activity coefficients of FeO, NiO, CoO, MoO_2 and MoO_3 in silicate melts, and its implications for trace element partitioning. *Chemical Geology* **186**, 151–181.

O'neill, H.C. & Berry, A.J. 2006. Activity coefficients at low dilution of CrO, NiO and CoO in melts in the system CaO-MgO-Al_2O_3-SiO_2 at 1400°C using the thermodynamic behavior of transitional metal oxides in silicate melts to probe their structure. *Chemical Geology* **231**, 77–89.

Pamić, J., Tomjlenović, B. & Balen, D. 2002. Geodynamic and petrogenetic evolution of Alpine ophiolites from central and NW Dinarides: an overview. *Lithos* **65**, 113–142.

Perfit, M.R., Gust, D.A., Bence, A.E., Arculus, R.J. & Taylor, R.S. 1980. Chemical characteristics of island-arc basalts: implications for mantle sources. *Chemical Geology* **30**, 227–256.

Presnall, D.C., Dixon, S.A., Dixon, J.R., O'donell, T.H., Brenner, N.L., Schrock, R.L. & Dycus, D.W. 1978 Liquidus phase relation on the join diopside-forsterite-anorthite from 1 atm to 20 kbar: their bearing on the generation and crystallization of basaltic magma. *Contribution to Mineralogy and Petrology* **66**, 203–220.

Rapien, M.H., Bodnar, R.J., Simmons, S.F., Szabó, Cs., Wood, C.P. & Sutton, S.R. 2003. Melt inclusion study of the embryonic porphyry copper system at White Island, New Zealand. *In*: Simmons, S.F. & Graham, I. (eds), *Volcanic, Geothermal, and Ore-Forming Fluids: Rulers and Witnesses of Processes within the Earth* (Werner F. Giggenbach Tribute) (ISBN 1-887483-90-X), Geochemical Society Special Publication Series **8**, Washington, D.C., 41–59.

Righter, K., Leeman, W.P. & Hervig, R.L. 2006. Partitioning of Ni, Co and V between spinel-structured oxides and silicates melt: importance of spinel composition. *Chemical Geology* **227**, 1–25.

Robertson, A.H.F. & Shallo, M. 2000. Mesozoic–Tertiary tectonic evolution of Albania in its regional Eastern Mediterranean context. *Tectonophysics* **316**, 197–254.

Roedder, E. 1984. *Fluid Inclusions. Reviews in Mineralogy* **12**. Mineralogical Society of America.

Roedder, E. 1987. Silicate liquid immiscibility in magmas. *In*: Yoder, H.S. (ed), *The Evolution of the Igneous Rocks*. Princeton University Press, Princeton, 15–58.

Sadofsky, S.J., Portnyagin, M., Hoernle, K. & Van Den Bogaard, P. 2008. Subduction cycling of volatiles and trace elements through the Central American Volcanic Arc: evidence from melt inclusions. *Contribution to Mineralogy and Petrology* **155**, 433–456.

Satari, P., Brenan, J.M., Horn, I. & Mcdonough, W.F. 2002. Experimental constraints on the sulfide- and chromite-silicate melt partitioning behavior of rhenium and platinum-group elements. *Economic Geology* **97**, 385–398.

Schiano, P. & Clocchiatti, R. 1994. Worldwide occurrence of silica rich melts in sub-continental and sub-oceanic mantle minerals. *Nature* **368**, 621–624.

Shallo, M. 1992. Geological evolution of the Albanian ophiolites and their platform periphery. *Geologische Rundschau* **81**, 681–694.

Shallo, M. 1994. Outline of the Albanian ophiolites. *Ofioliti* **19**, 681–694.

Sun, S.S. & McDonough, W.F. 2002. Chemical and isotopic systematics of oceanic basalts: implications for mantle composition and progress. *In*: Saunders, A.D. & Norry, M.J. (eds), *Magmatism in Oceanic Basins*. Geological Society, London, Special Publications **42**, 313–345.

Sharygin, V.V., Szabó, C., Kóthay, K., Timina, T.J.U., Pető, M., Török, K., Vapnik, Y.E. & Kuzmin, D.V. 2007. Rhönite in silica-undersaturated alkali basalts: inferences on silicate melt inclusions in olivine phenocrysts. Alkaline magmatism, its sources and plumes. Irkutsk-Napoli, *In*: Vladykin, N.V. (ed), *Vinogradov Institute of Geochemistry*, 157–182.

Sobolev, A.V. 1996. Melt inclusions in minerals as a source of principle petrological information. *Petrology* **4/3**, 228–239.

Spandler, C., O'neill, H.S. & Kamenetsky, V. 2007. Survival times of anomalous melt inclusions from element diffusion in olivine and chromite. *Nature* **447**, 303–306.

Watson, E.B. 1976. Glass inclusions as sample of early magmatic liquid: determinative method and application to a South Atlantic basalt. *Journal of Volcanology and Geothermal Research* **1**, 73–84.

Webster, J.D. & Rebbert, C.R. 2001. The geochemical signature of fluid-saturated magma determined from silicate melt inclusions in Ascension Island granite xenoliths. *Geochimica et Cosmochimica Acta* **65**, 123–136.

Zajacz, Z., Kovács, I., Szabó, Cs., Halter, W. & Pettke, T. 2007. Evolution of mafic alkaline melts crystallized in the uppermost lithospheric mantle: a melt inclusion study of olivine-clinopyroxenite xenoliths, Northern Hungary. *Journal of Petrology* **48**, 853–883.